Damping Values Derived from Surface-Source, Downhole-Receiver Measurements at 22 Sites in the San Francisco Bay Area of Central California and the San Fernando Valley of Southern California

David M. Boore[*1], James F. Gibbs[2,†], and William B. Joyner[2,‡]

ABSTRACT

A method discussed in Gibbs, Boore, *et al.* (1994) was applied to surface-source, downhole-receiver recordings at 22 boreholes, in the San Francisco Bay area in central California and the San Fernando Valley of southern California, to determine the average damping ratio of shear waves over depth intervals ranging from about 10 m to as much as 245 m (at one site), with most maximum depths being between 35 and 90 m. The average damping values range from somewhat less than 1% to almost 8%, with little dependence on grain size for sites in sediments. Surprisingly, the average damping values for sites with average velocities greater than about 450 m/s, including, but not limited to rock sites, are generally larger than for sites with lower average velocities. The combined effect of the higher damping and shorter travel times through the rock columns, however, leads to an effective attenuation that is generally comparable or smaller than for soil sites.

KEY POINTS

- Damping values from boreholes, using surface sources and downhole receivers, are determined for 22 sites.
- The average damping values range from less than 1% to almost 8%, with little dependence on grain size.
- The damping values are important in predictions of strong ground motion amplitudes.

Supplemental Material

INTRODUCTION

Gibbs, Boore, *et al.* (1994; hereafter, Gea94) discussed two methods for extracting effective damping values from recordings in boreholes from a repeatable shear-wave surface source. One method used the ratio of Fourier spectra at two depths, and the other used the change in Fourier spectral amplitudes as a function of depth for individual frequencies. In Gea94, the methods were applied to recordings at a site near Gilroy, in central California. Subsequent to the publication of Gea94, the second method was applied to 22 sites in the San Francisco Bay area (SFBA) and the San Fernando Valley (SFV) of southern California. This article gives damping values for these sites as well as the combined effect of the damping and the velocity structure through which earthquake waves would travel to reach the surface at the sites.

The data collection and the bulk of the analysis were done by the second author, using revised computer programs prepared primarily by the third author. The analysis was done before the second and third authors retired. The first author was substantially involved in analysis reported in Gea94 and in a later paper (Boore *et al.*, 2003) that applied the method used in the current article to data collected by the second author at one of the 22 sites discussed here. He was also involved in numerous discussions regarding the work. For reasons no longer remembered, a paper describing the results for all 22 sites presented here was not prepared, even in draft form,

1. Scientist Emeritus, U.S. Geological Survey, Earthquake Science Center, Menlo Park, California, U.S.A.; 2. U.S. Geological Survey, Earthquake Science Center, Menlo Park, California, U.S.A.

*Corresponding author: boore@usgs.gov

†Deceased (2019).

‡Deceased (2001).

Cite this article as Boore, D. M., J. F. Gibbs, and W. B. Joyner (2020). Damping Values Derived from Surface-Source, Downhole-Receiver Measurements at 22 Sites in the San Francisco Bay Area of Central California and the San Fernando Valley of Southern California, *Bull. Seismol. Soc. Am.* **111**, 2158–2166, doi: 10.1785/0120200225

before the deaths of the second and third authors. But files of results were given to the first author, who was able to reconstruct the analysis steps and interpret the results of the earlier analyses. Unfortunately, all of the original digital data from decades ago are not available, precluding some analyses that might be informative, but such analyses would not change the basic results in this article.

METHOD

The method is described in Gea94 and also in Boore *et al.* (2003, pp. 2741–2743). Using what is somewhat different terminology, but following Gea94, the Fourier spectral amplitude $A(f, z)$ at a frequency f from a surface source recorded on a borehole receiver at a depth z is adjusted for both geometrical spreading and the changes in amplitude produced by impedance effects ($G(z)$), and the adjusted amplitude $A'(f, z) = G(z)A(f, z)$ is related to the attenuation due to propagation from the surface source to a receiver in the borehole by this equation:

$$A'(f, z) = F \exp(-\pi f t^*(z)), \tag{1}$$

in which F is a factor that includes contributions from the source, the coupling of the downhole seismometer to the borehole casing, and wave propagation distortions, such as reverberations within layers. As discussed in Gea94, F is assumed to be a function of frequency but not depth. Any depth effects not included in the adjustment factor $G(z)$ are accounted for using synthetic seismograms, as discussed later. In equation (1)

$$t^*(z) = \int_0^{l(z)} Q^{-1}(l) V_S^{-1}(l) dl, \tag{2}$$

and the integral is taken over the path l taken between the surface source and the downhole receiver; the path is an implicit function of depth. The amount of attenuation due to processes such as anelastic attenuation and scattering is parameterized by Q—the measure of attenuation most often used in seismology. Because the cumulative attenuation is an integral over the inverse of Q, however, we prefer to use the damping ratio as the measure of attenuation. This measure of attenuation, commonly used in engineering, is often represented by the Greek letter ξ, but we have chosen the more familiar symbol D. The damping ratio D is related to Q by the following equation:

$$D = 0.5/Q. \tag{3}$$

We use D as an overall measure of damping, not just the intrinsic damping that is measured from small samples in the laboratory.

Following Gea94 and Boore *et al.* (2003), we assume that the damping ratio is independent of travel path, such that equations (2) and (3) become

$$t^*(z) = 2D_{\mathrm{AVG}}\tau(z), \tag{4}$$

in which $\tau(z)$ is the travel time between the surface and a receiver at depth z. The travel time in equation (4) is given by

$$\tau(z) = \int_0^z V_S^{-1}(l) dl. \tag{5}$$

We chose to derive an average damping over a range of depths, rather than a depth-dependent damping, because the change in amplitude from one recording depth to another, due to attenuation, is small compared with the variability in the measurements, thus making it difficult to obtain reliable estimates of the depth dependence of damping. We added the subscript "AVG" to D, to indicate that the derived damping is an average value over a range of depths. Replacing the point-wise attenuation properties with a quantity that represents the cumulative effect of propagating over a depth range is similar to the use of the attenuation parameter κ in simplified site-response calculations (e.g., Boore, 2013), using the following equation:

$$\text{Attenuation} = \exp(-\pi f \kappa). \tag{6}$$

This is the same as equation (1), except for using κ rather than t^* as the attenuation parameter. Campbell (2009) has a discussion of the different parameters, in which he points out that t^* can be frequency dependent, whereas by the definition of Anderson and Hough (1984), κ is frequency independent. Another difference between t^*, as used here, and κ is that $t^*$is a measure of attenuation over a specified depth range for waves from an active surface source recorded in a borehole, whereas κ is usually a measure of the cumulative attenuation from an earthquake source and a site. κ is usually dependent on source-to-site distance R; κ_0, frequently used in simulations of ground motion, is an approximation of the zero distance intercept of $\kappa(R)$. It is widely assumed that κ_0 represents the attenuation over the last few kilometers of propagation, but the distance over which this attenuation occurs is indeterminate, unlike t^* as used here.

From equations (1) and (4),

$$\ln(A'(f, z)) = \ln(F) - 2\pi f D_{\mathrm{AVG}}\tau(z). \tag{7}$$

For a single frequency f, the average damping can be obtained from the slope of a line fit to $\ln A'$ versus τ. This is the second of the two methods discussed in Gea94 (the first uses spectral ratios from two depths); an example of the regression and the points being fit is given in Figure 1. A straight line is a good fit to $\ln A'$ over the range of depths, particularly for depths greater than 15 m, thus providing some justification for the use of a constant damping ratio over a range of depths. A modification made subsequent to Gea94 is to find period-independent values of D_{AVG} by minimizing the sum of squares of residuals relative to a reference frequency (in effect, using equation 7 for a suite of frequencies, solving for the constant D_{AVG}).

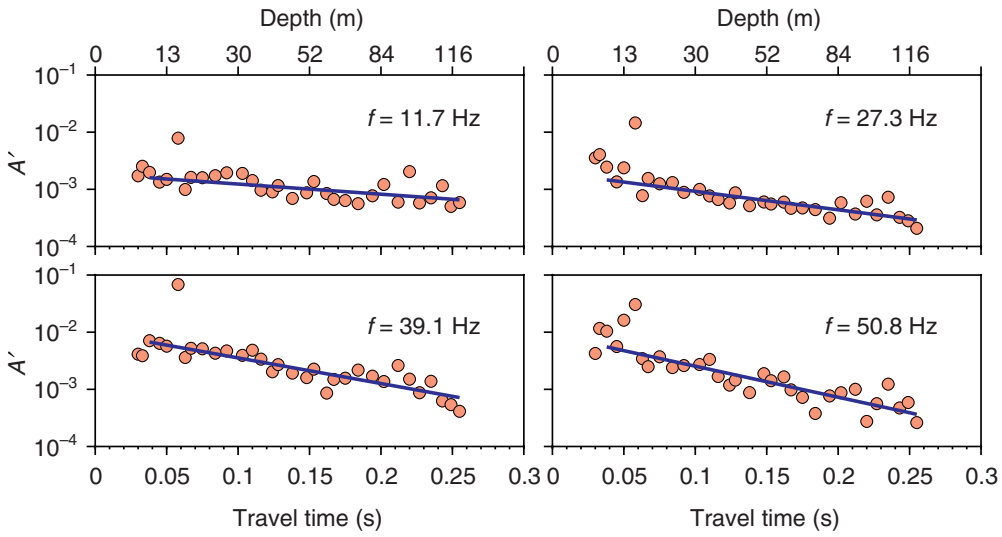

Figure 1. Spectral amplitude (A) adjusted for geometrical spreading and impedance changes (G), as a function of travel time for the GIL2 borehole, for a subset of the frequencies used in Gibbs, Boore *et al.* (1994; hereafter, Gea94), ranging from almost the lowest to the highest frequencies, with two intermediate frequencies. The damping values were derived from the slope of the line fit to the log of the adjusted amplitude versus travel time, starting at a depth of 7.5 m and excluding the outlier at a depth of 15 m (modified from fig. 9 in Gea94). The color version of this figure is available only in the electronic edition.

As discussed in Gea94 and Boore *et al.* (2003), synthetic seismograms that include all multiple reverberations were generated for the velocity profile at each site and a specified value of D_{AVG}. One important reason for using the synthetic seismograms is to correct for the approximations used in computing the adjustment factor $G(z)$; the computation of $G(z)$ is described in Gea94.$G(z)$ is strongly dependent on the shear-wave velocity profile and can be quite large, as shown in figure 7 in Gea94. The shear-wave velocity profiles are well determined (as can be determined from the information included in the supplemental material to this article) and are not a source of significant uncertainty in the calculation of $G(z)$. The

TABLE 1
Site Information

Region	Site	Site Name	Latitude (°)	Longitude (°)	D2Bot*	V_{S30} (m/s)	Hoff†	References
SFV	ELC	Epiphany Lutheran Church	34.2117	−118.6051	83.5	267.5	4	Gibbs *et al.* (1999)
SFV	I10	La Cienega	34.0364	−118.3771	249.5	269.0	5	Boore *et al.* (2003)
SFV	JGB	Jensen Generator Building	34.3130	−118.4983	89.5	525.8	4	Gibbs *et al.* (1999)
SFV	JMB	Jensen Main Building	34.3111	−118.4957	89.5	373.1	5	Gibbs *et al.* (1999)
SFV	KES	Knolls Elementary School	34.2633	−118.6664	67.5	557.4	4	Gibbs *et al.* (1999)
SFV	LAD	Los Angeles Dam	34.2931	−118.4839	88.5	629.0	4	Gibbs *et al.* (1999)
SFV	OVH	Olive View Hospital	34.3281	−118.4442	89.5	440.5	4	Gibbs *et al.* (1999)
SFV	RIN	Rinaldi Receiving Station	34.2810	−118.4771	79.5	332.8	4	Gibbs *et al.* (1999)
SFV	SCW	Sylmar Converter West	34.3117	−118.4893	87.0	251.2	4	Gibbs *et al.* (1999)
SFV	SOP	Sherman Oaks Park	34.1607	−118.4394	89.5	301.6	4	Gibbs *et al.* (1999)
SFV	SOW	Sherman Oaks Woodman	34.1543	−118.4307	89.5	257.6	4	Gibbs *et al.* (1999)
SFV	SVA	Sepulveda VA Hospital	34.2490	−118.4772	74.5	365.0	4	Gibbs *et al.* (1999)
SFV	WOC	White Oak Church	34.2081	−118.5171	89.5	280.9	4	Gibbs *et al.* (1999)
SFBA	APT	Hollister Airport	36.8892	−121.4111	59.4	215.5	4	Gibbs and Fumal (1994)
SFBA	BPB	Beach Park Blvd	37.5558	−122.2467	90.0	126.4	1.3	Gibbs, Fumal, and Powers (1994)
SFBA	CVR	Calaveras Reservoir	37.4529	−121.8068	57.1	477.9	4	Gibbs and Fumal (1994)
SFBA	FMT	Fremont	37.5353	−121.9300	45.0	284.8	4	Gibbs, Fumal, and Powers (1994)
SFBA	GIL2	Gilroy number 2 (USGS)	36.9817	−121.5549	196.7	296.8	5	Gibbs *et al.* (1992)
SFBA	PGC	Presidio Golf Course	37.7912	−122.4580	54.6	594.5	4	Gibbs *et al.* (1993)
SFBA	SCA	Sunnyvale Colton Avenue	37.4028	−122.0248	60.0	267.7	3	Gibbs, Fumal, and Powers (1994)
SFBA	SFO	San Francisco International Airport	37.6221	−122.3981	145.0	224.7	5	Gibbs *et al.* (1992)
SFBA	TRI	Treasure Island	37.8256	−122.3729	100.0	172.1	4	Gibbs *et al.* (1992)

SFBA, San Francisco Bay area; SFV, San Fernando Valley; USGS, U.S. Geological Survey.
*Depth to bottom of borehole, in meters.
†Horizontal offset distance from the source to the borehole, in meters.

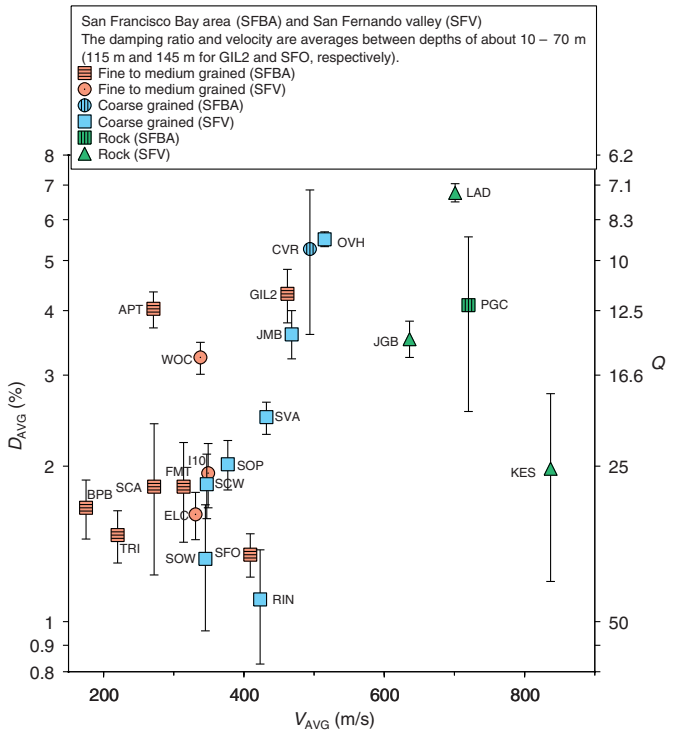

Figure 2. Damping values averaged over a depth range from about 8 to 70 m (some sites did not provide data to 70 m, as shown in a later figure), as a function of average velocity (calculated as z_{AVG} divided by the travel time from the surface to that depth). The bars are 68% confidence intervals, determined from the uncertainty of the slope in the fit of equation (7) to the data. The same is true for the bars in subsequent figures. The color version of this figure is available only in the electronic edition.

surface source used to produce the waves recorded in the boreholes has a dimension of 2.3 m and is oriented perpendicular to a line from the source to the borehole, offset from the borehole by a distance given by hoff in Table 1. The offset distance is included in calculations of $G(z)$, although Gea94 find that the differences in $G(z)$ computed for a source offset from the borehole and a source directly over the borehole are only important for the shallowest depths. The synthetic data were analyzed in the same way as the observations, and the ratio of the derived D_{AVG} to the specified D_{AVG} was used as a correction factor for the damping derived from the data. This correction factor was generally small (on the order of a few tens of a percent or less; an example can be seen in fig. 8 of Gea94.).

RESULTS

The method discussed earlier was applied to data obtained in boreholes from an active shear-wave surface source. The details of the data collection are given in Gea94. New to this article are data from 22 sites in the SFBA of central California and the SFV of southern California (with one site—I10—being in the Los Angeles basin, just south of the SFV). Site information is given in Table 1; borehole recordings were obtained at a depth spacing of 2.5 m. The average shear-wave damping D_{AVG} was computed from equation (7), in which the line was fit to data over depth intervals ranging from about 10 m (as chosen on a site-by-site basis, according to the quality of the data) to the lesser of either the greatest depth at which data were collected or 70 m. Strictly speaking, D_{AVG}represents the average damping ratio between the two depths used in fitting equation (7) to the data. The deeper depth is represented as z_{AVG}. The depth of about 10 m was chosen to avoid complications due to the finite offset of the source, in which the paths traveling between the surface source and the shallowest receivers might be different than if the source was directly above the borehole. The shallow depth of about 10 m used in fitting the equation (7) to the data also avoided divergences of the near-surface measurements from the linear fit to $\ln A'$ versus the travel time. The depth of about 70 m was chosen to provide a deepest depth that is shared by most boreholes, while avoiding the increasing noise in the data at deeper depths. Results are shown in Figure 2 for the two regions. The damping values presented in this article were derived from the frequency-independent modification to the second Gea94 method. For purposes of the plot, the abscissa in Figure 2 is the time-average velocity from the surface to z_{AVG}, given by

$$V_{AVG} = \frac{z_{AVG}}{\tau(z_{AVG})}, \tag{8}$$

in which τ is the vertical travel time from the surface to z_{AVG}, given by equation (5). The actual average velocity between the depth of about 10 m and z_{AVG} would generally be somewhat greater than given by equation (8), but not enough to alter the conclusions of this article. The lithologic descriptions shown in Figure 2 are subjective judgements made by the second author from the geologic logs presented in the various reports referenced in Table 1 (for the convenience of the reader, these logs have been collected in the supplemental materials). As there is often a mix of fine- and coarse-grained layers, the assignment into one of three groups is a simplification of reality.

In comparing the results for the various sites, it should be kept in mind that the data collection and analysis procedures were the same for all sites. The damping values from both regions are comparable for similar values of the average velocity. With two exceptions (APT and WOC), the damping values for slower sites (less than about 400 m/s) are generally consistent with one another, with damping values around 1.7% (corresponding to an average Q of 30). Not surprisingly, there is a correlation between grain size and velocity, with finer grained sediments having slower velocities than coarser grained sediments, but there seems to be no dependence of the average damping values on grain size.

For some of the sites, average damping and velocity estimates were made for several values of z_{AVG}. To provide some idea of the importance of the averaging interval, Figure 3 shows the average damping as a function of z_{AVG}. Some of the sites

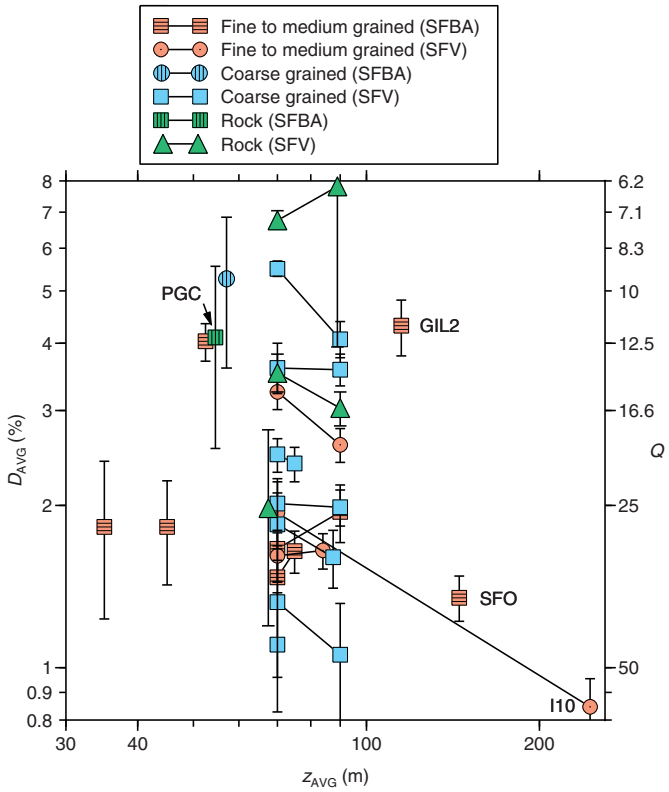

Figure 3. Damping values averaged over a depth range from about 10 m to z_{AVG}. For some sites the results are only available for a single value of z_{AVG}, and for other sites the results are available for two values of z_{AVG}, with slanted lines connecting the two values of damping for the same site. The bars are 68% confidence intervals. The color version of this figure is available only in the electronic edition.

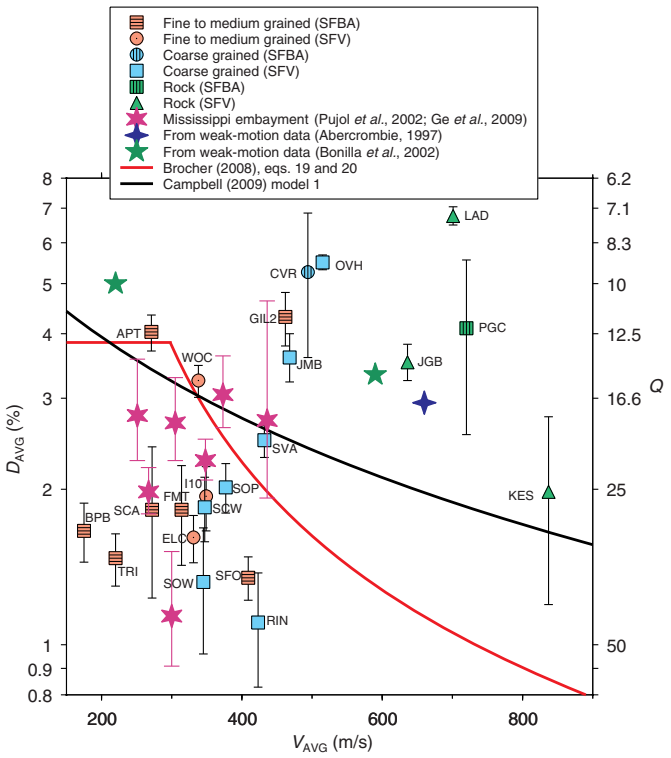

Figure 4. Comparison of measured damping values from both the San Fernando Valley (SFV) and the San Francisco Bay area (SFBA), damping values from other areas, and selected relations for soil sites. The bars are 68% confidence intervals. The color version of this figure is available only in the electronic edition.

had average damping values for two depths; the values for these sites are connected by lines. With one exception (I10), for those sites with damping values at two depths, there is not enough range in the averaging depths to draw firm conclusions about the depth dependence of the average damping value. The I10 results, however, show a clear decrease in average damping with increasing depth, which is not surprising, because most of the attenuation will probably be from lower-velocity shallower layers where the waves spend more time than in the faster velocity deeper layers; averaging over deeper layers that produce little attenuation in the waves traveling through the layers will result in a lower D_{AVG} from the surface to depth.

DISCUSSION

To see how our damping values compare with those from other researchers, Figure 4 is a repeat of Figure 2, with values from several studies used in Campbell (2009) and a few damping-velocity curves added to the figure. All of the damping values are for shear waves. The added damping values from the Mississippi embayment (Pujol *et al.*, 2002; Ge *et al.*, 2009) used measurements and an interpretation method similar to Gea94 (active surface source and downhole receivers). The other two sources of damping values in Figure 4 used weak-motion recordings from earthquakes. As Campbell (2009) discusses, there are differences in frequency content between the two types of observations, with weak-motion recordings being lower frequency than the surface-source, downhole-receiver records. As an aside, the attenuation parameter κ_0, commonly used in simulations of strong ground motion, is often derived from ground-motion data at frequencies ranging from about 10 to 25 Hz (e.g., Ktenidou *et al.*, 2014; Cabas *et al.*, 2017), which overlaps the 12–58 Hz range of frequencies used in our determinations of the damping value.

For comparison, low-strain damping ratios from laboratory measurements are generally in the range of 1%–2%, with somewhat higher values for coarser soils (up to 3.5% for gravels) (Electric Power Research Institute, 1993) and vary little with frequency of vibration and plasticity index (Darendelli, 2001). These values are consistent with our values for soils, and, given that the laboratory measurements do not include the effects of scattering, suggest that our results are more representative of intrinsic damping than the combined effect of damping and scattering, at least, for the sites with V_{AVG} less than about 450 m/s.

The Brocher and Campbell curves in Figure 4 provide a convenient basis for discussion, although it should be kept in mind that the curves were derived from damping and velocity relations as a function of depth, and do not represent averages of the damping and velocity over ranges of depth, as is the case for the observations. Therefore, the relation between the curves and the observations is only a convenient and qualitative comparison (converting them to averages over depth would require the choice of a representative velocity profile, but the basic conclusion drawn by comparing the derived damping values with the curves would not change). There are two obvious differences in the relation of the damping values and the curves: (1) most of the observed damping values for slower average velocities fall below those curves (including the values from the Mississippi embayment, which are consistent with the values reported in this article), and (2) at higher average velocities, the damping values are above the curves.

Campbell (2009) recognized the different relations between the published damping values and the curves for low and high velocities. Regarding point 1 in the previous paragraph, he observed that the low damping values are predominately from what he calls "seismic survey data" (generally from surface-source, downhole-receiver receiver measurement, as in this article), and might be predominately a measure of intrinsic damping and not include the effect of scattering. But note from Figure 4 that for the sites with V_{AVG} less than about 450 m/s, APT and WOC have damping values higher than the values at the other sites and similar to that derived from the weak-motion data, even though the damping values at those two sites used the same measurement and interpretation methods as the more numerous sites with lower damping values.

SFO and GIL2 form an interesting pair, in that they have similar average velocities and depths, but very different damping values (see Figs. 3 and 4). They are both given a "fine-to-medium grained" classification, but according to the geologic logs in the open-file reports referenced in Table 1 (the geologic logs are provided in the supplemental materials), SFO, which has one of the lowest damping values for this category, is mostly sand in the underlying sediments, whereas GIL2, which has one of the highest damping values for this category, is a mix of clay, sandy loam, and gravel layers. It could be that the detailed lithology is important in controlling the damping values, but that the two soil categories used in the figures are too coarse to be useful in capturing the dependence of the damping values on the lithology underlying the sites.

The damping values for most sites with average velocities greater than about 450 m/s are larger than for most of the slower velocity sites. This includes the few available rock sites (with the exception of KES). Our damping values for the higher velocity sites are somewhat similar to those from the two weak motion values shown in Figure 4 (an average of about 4.3% for our values and 3.1% for the weak motion values). It might seem suspicious that the average damping values for coarse-grained sites increase suddenly, at velocities above about 450 m/s. We know of no reason to suspect the measurements or the analysis, and the measurement and analysis methods, as well as the frequencies of motions, are the same for all of our sites. The high values cannot be explained as a result of geographic variation, as two of the highest values are from sites (CVR and OVH) in the SFBA and the SFV. It could be that the fractures in the rock-like sites lead to more scattering than for softer sites, such that the measured damping includes contributions from intrinsic and scattering damping. A reviewer suggested that this could be tested by looking for differences in Poisson's ratio for different groups of sites, for depths above the water table. We made graphs of average Poisson's ratios as a function of depth for two sets of boreholes: (1) V_{AVG} less than and greater than 450 m/s, and (2) D_{AVG} less than and greater than 3.0%. Unfortunately, the depths to the water table (as estimated by the depth to a P-wave velocity of 1500 m/s) were so shallow that meaningful differences in Poisson's ratios could not be determined for the depths of the most interest (greater than about 20 m).

The conclusion that faster sites have greater damping seems nonintuitive. Most relations between point values of velocity and Q show a decreasing damping, with increasing velocity (e.g., Brocher, 2008a,b). But the high damping values for rock sites does not necessarily mean that the effective attenuation of waves passing through the rock columns will be greater than for waves traveling through soil layers. As equation (7) shows, the attenuation is determined by the damping value and by the travel time through the material. The waves will spend less time traveling through rock materials than soil materials, and, this will tend to offset the greater damping values found in this study, for faster sites. To see the effect of this trade-off, t^* was computed from equation (4), assuming that the waves travel vertically from the depth z_{AVG} to the surface and that the damping value D_{AVG} applies to the same depth range (even though the values generally apply to materials deeper than about 10 m). The results are shown in Figures 5 and 6, which should be compared with Figures 2 and 3. Although the overall range of t^* and D_{AVG} values is about the same (a factor of 6), it is clear that the combined effect of attenuation and propagation has reduced the difference between soil and rock sites, sometimes drastically (e.g., PGC in Figs. 5 and 6, a site underlain by serpentine of the Franciscan formation).

Also included in Figure 6 are attenuation measurements from earthquake motions measured at stations of the KiK-net network (Xu *et al.*, 2020). The attenuation measurements are differences in κ measured by fitting lines to plots of the logarithm of the Fourier spectra versus frequency, from recordings at the surface and at the bottom of the KiK-net borehole. The difference in κ is called $\Delta\kappa_0$ by Xu *et al.* (2020). Because the Xu *et al.* (2020) values were determined using the classical method of Anderson and Hough (1984), I have retained their terminology in the legend to Figure 6.

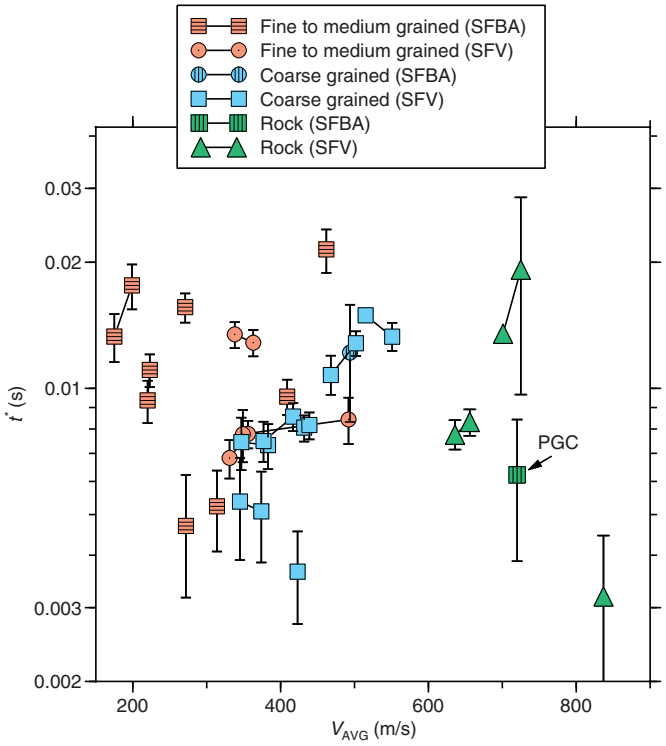

Figure 5. t^* versus V_{AVG} for the SFV and the SFBA. Lines connect values derived from damping values determined from two z_{AVG} depths, when available. The bars are 68% confidence intervals. The color version of this figure is available only in the electronic edition.

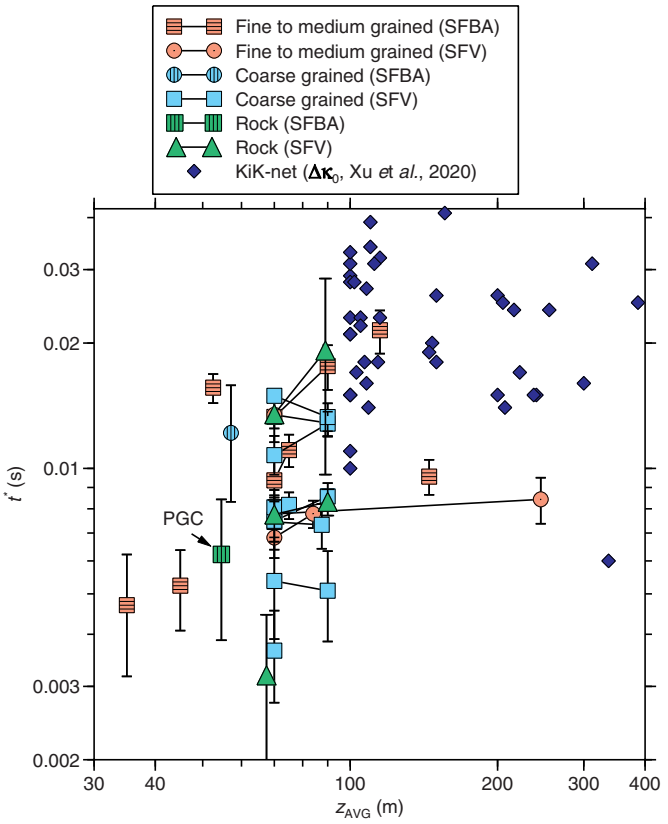

Figure 6. t^* versus z_{AVG} for the SFV and the SFBA. Lines connect values derived from damping values determined from two z_{AVG} depths, when available. For comparison, values of $\Delta\kappa_0$ from KiK-net boreholes in Japan are also shown. The bars are 68% confidence intervals. The color version of this figure is available only in the electronic edition.

The values from this article used a completely different method and a different source of the waves, and I have kept the t^* terminology for those measurements, although the effect on cumulative attenuation is given by similar equations (equations 1 and 6). As shown in Figure 6, the $\Delta\kappa_0$ values are generally larger than the t^* values, but they also represent the effective attenuation over a larger depth range than used for t^*. For this reason, it is tempting to conclude that the combined set of values demonstrates a depth dependence to the overall attenuation, with less cumulative attenuation for shallower averaging depths. This makes intuitive sense, but two of the three t^* obtained for depths greater than 100 m are less than all but one $\Delta\kappa_0$ for the same depths. This might be because of geographical differences in the sediment profiles or because of different mixes of intrinsic versus scattering attenuation.

As was done in Figures 5 and 6, the damping values can be combined with the velocity models to compute the effective attenuation of waves traveling from z_{AVG} to the surface. For the non-rock sites, this would be useful if z_{AVG} always corresponded to the thickness of the sediments above rock. But cost considerations resulted in most of the boreholes being drilled to shallower depths, before the underlying rock was encountered. The two exceptions are the boreholes at TRI and OVH, which entered rock near the bottom of the boreholes (see the geologic logs in the supplemental materials). More attenuation can be expected in materials below z_{AVG}, so the t^* values should be considered minimum values of the attenuation parameter. The values of t^* in Figures 5 and 6 are generally much less than the κ or κ_0 values found in many studies from surface measurements at sites with average velocities similar to the sites used in this article, which have a minimum value of about 0.02 s (e.g., fig. 10 in Van Houtte *et al.*, 2011; fig. 9 in Cabas *et al.*, 2017; and fig. 5 in Xu *et al.*, 2020). This is not surprising, as the κ_0 values in those references include contributions from attenuation below the near-surface materials. It would be surprising if our values were higher than the values in the cite references; that would be an inconsistency suggesting problems with our measurements or analysis method.

Limitations and drawbacks

This article presents in situ damping measurements that have not been presented before, but the limited depth ranges for the measurements mean that the damping ratios should not be

used as-is in site-response calculations. Our results, however, can provide guidance in the development of damping versus depth distributions, as was done by Campbell (2009), who used damping values from other parts of the country obtained using methods and depth ranges similar to those in this article. One obvious potential drawback to using the damping values presented in this article in ground-motion simulations is that the measurements are at frequencies generally higher (greater than 10 Hz) than the lower frequencies of most interest in engineering applications. As shown in figure 10 of Gea94 and figure 6 of Boore *et al.* (2003), a frequency dependence to the damping values is sometimes observed, but the lack of energy from the surface source at lower frequencies makes it hard to determine reliable damping values at low frequencies.

SUMMARY

Damping values averaged over depths ranging from 35 to 245 m have been obtained from 22 boreholes in the SFV and the SFBA. The values have been obtained from surface-source, downhole-receiver measurements, collected and analyzed in the same way for all boreholes. For averaging depths down to 70 m, the results show minimal dependence of the damping values on the types of soils, with damping values ranging from 1.3% to 4.3% for fine- to medium-grained sediments and 1.1% to 5.5% for coarse-grained sediments. There seems to be a dependence of the damping values on the shear-wave velocity averaged from the surface to the depths used in determining the average damping values. Surprisingly, the damping values for lower-average-velocity sites are lower than for higher-average-velocity sites, including rock sites. For sites with average velocities less than 450 m/s, the damping values range from 1.1% to 4.0%, with most values near 2%. For higher-average-velocity sites, the values range from 2.0% to 6.8%. This dependence is largely removed when the effective attenuation, which depends both on the damping values and the shear-wave velocity, is computed.

DATA AND RESOURCES

The borehole recordings used in this article are shown in record sections in the references for each borehole, as given in Table 1. The simulated motions were obtained from R. Herrmann's HSPEC91 program, and the graphs were prepared using CoPlot (www.cohort.com, last accessed September 2020). Portable document format (pdf) files containing geologic logs of the 22 boreholes, taken from the individual references for each borehole, are contained in the supplemental material. In addition, the supplemental material contains graphs relevant to the derivation of the *S*-wave velocity model for each borehole.

ACKNOWLEDGMENTS

The authors thank Robert E. Westerlund for his help in the field, Hsi-Ping Liu and Robert E. Westerlund for designing and building the shear-wave hammer, Robert B. Herrmann for providing his wave-propagation program HSPEC91 and for spending time with the first author (David M. Boore) in Menlo Park, helping him with that program, and Ellen Rathje for providing data appearing in the Xu *et al.* (2020) paper. This article was improved by incorporating Ken Campbell's useful comments on an earlier version. The first author also thanks Ashly Cabas, Shane Detweiler, Harry Jenter, Keith Knudsen, Charles Mueller, Eric Thompson, and two anonymous reviewers for comments that improved this article. Any use of trade, firm, or product names is for descriptive purposes only and does not imply endorsement by the U.S. Government.

REFERENCES

Abercrombie, R. A. (1997). Near-surface attenuation and site effects from comparison of surface and deep borehole recordings, *Bull. Seismol. Soc. Am.* **87,** 731–744.

Anderson, J. G., and S. E. Hough (1984). A model for the shape of the Fourier amplitude spectrum of acceleration at high frequencies, *Bull. Seismol. Soc. Am.* **74,** 1969–1993.

Bonilla, L. F., J. H. Steidl, J. C. Gariel, and R. J. Archuleta (2002). Borehole response studies at the Garner Valley downhole array, southern California, *Bull. Seismol. Soc. Am.* **92,** 3165–3179.

Boore, D. M. (2013). The uses and limitations of the square-root impedance method for computing site amplification, *Bull. Seismol. Soc. Am.* **103,** 2356–2368.

Boore, D. M., J. F. Gibbs, W. B. Joyner, J. C. Tinsley, and D. J. Ponti (2003). Estimated ground motion from the 1994 Northridge, California, earthquake at the site of the interstate 10 and La Cienega Boulevard bridge collapse, west Los Angeles, California, *Bull. Seismol. Soc. Am.* **93,** 2737–2751.

Brocher, T. M. (2008a). Compressional and shear-wave velocity versus depth relations for common rock types in northern California, *Bull. Seismol. Soc. Am.* **98,** 950–968, doi: 10.1785/0120060403.

Brocher, T. M. (2008b). Key elements of regional seismic velocity models for long period ground motion simulations, *J. Seismol.* **12,** 217–221.

Cabas, A., A. Rodriguez-Marek, and L. F. Bonilla (2017). Estimation of site-specific kappa (κ_0)-consistent damping values at KiK-net sites to assess the discrepancy between laboratory-based damping models and observed attenuation (of seismic waves) in the field, *Bull. Seismol. Soc. Am.* **107,** 2258–2271.

Campbell, K. W. (2009). Estimates of shear-wave Q and κ_0 for unconsolidated and semiconsolidated sediments in eastern North America, *Bull. Seismol. Soc. Am.* **99,** 2365–2392.

Darendelli, M. B. (2001). Development of a new family of normalized modulus reduction and material damping curves, *Ph.D. Thesis*, The University of Texas at Austin, 362 pp.

Electric Power Research Institute (1993). *Guidelines for determining design basis ground motions*, *Final Report, EPRI TR-102293*, Palo Alto, California.

Ge, J., J. Pujol, S. Pezeshk, and S. Stovall (2009). Determination of shallow shear-wave attenuation in the Mississippi embayment using vertical seismic profiling data, *Bull. Seismol. Soc. Am.* **99,** 1636–1649.

Gibbs, J. F., and T. E. Fumal (1994). *Seismic velocities and geologic logs at seven strong-motion stations that recorded the 1989 Loma Prieta, California, earthquake, Part IV*, *U.S. Geol. Surv. Open-File Rept. 94-552*, 91 pp.

Gibbs, J. F., D. M. Boore, W. B. Joyner, and T. E. Fumal (1994). The attenuation of seismic shear waves in Quaternary alluvium in Santa Clara Valley, California, *Bull. Seismol. Soc. Am.* **84,** 76–90.

Gibbs, J. F., T. E. Fumal, D. M. Boore, and W. B. Joyner (1992). *Seismic velocities and geologic logs from borehole measurements at seven strong-motion stations that recorded the Loma Prieta earthquake*, *U.S. Geol. Surv. Open-File Rept. 92-287*, 139 pp.

Gibbs, J. F., T. E. Fumal, and T. J. Powers (1993). *Seismic velocities and geologic logs from borehole measurements at eight strong-motion stations that recorded the 1989 Loma Prieta, California, earthquake*, *U.S. Geol. Surv. Open-File Rept. 93-376*, 119 pp.

Gibbs, J. F., T. E. Fumal, and T. J. Powers (1994). *Seismic velocities and geologic logs from borehole measurements at seven strong-motion stations that recorded the 1989 Loma Prieta, California, earthquake*, *U.S. Geol. Surv. Open-File Rept. 94-222*, 104 pp.

Gibbs, J. F., J. C. Tinsley, D. M. Boore, and W. B. Joyner (1999). *Seismic velocities and geological conditions at twelve sites subjected to strong ground motion in the 1994 Northridge, California, earthquake: A revision of OFR 96-740*, *U.S. Geol. Surv. Open-File Rept. 99-446*, 142 pp.

Ktenidou, O. J., F. Cotton, N. A. Abrahamson, and J. G. Anderson (2014). Taxonomy of κ: A review of definitions and estimation approaches targeted to applications, *Seismol. Res. Lett.* **85,** 135–146.

Pujol, J., S. Pezeshk, Y. Zhang, and C. Zhao (2002). Unexpected values of Q_s in the unconsolidated sediments of the Mississippi embayment, *Bull. Seismol. Soc. Am.* **92,** 1117–1128.

Van Houtte, C., S. Drouet, and F. Cotton (2011). Analysis of the origins of κ (kappa) to compute hard rock to rock adjustment factors for GMPEs, *Bull. Seismol. Soc. Am.* **101,** 2926–2941.

Xu, B., E. M. Rathje, Y. Hashash, J. Stewart, K. Campbell, and W. J. Silva (2020). $\kappa_0$for soil sites: Observations from KiK-net sites and their use in constraining small-strain damping profiles for site response analysis, *Earthq. Spectra* **36,** 111–137.

Manuscript received 25 June 2020
Published online 3 November 2020